ACS APPLIED MATERIALS & INTERFACES

Research Article

www.acsami.org

Vertically Aligned ZnO Nanorods on Hot Filament Chemical Vapor Deposition Grown Graphene Oxide Thin Film Substrate: Solar Energy Conversion

Sadia Ameen,[†,‡] M. Shaheer Akhtar,[†,§] Minwu Song,[‡] and Hyung Shik Shin*[,‡]

[‡]Energy Materials & Surface Science Laboratory, Solar Energy Research Center, School of Chemical Engineering, Chonbuk National University, Jeonju, 561-756, Republic of Korea

[§]New & Renewable Energy Material Development Center (NewREC), Chonbuk National University, Jeonbuk, Republic of Korea

ABSTRACT: Vertically aligned zinc oxide (ZnO) nanorods (NRs) were grown by the low-temperature hydrothermal method on graphene oxide (GO) coated FTO substrates, where GO was directly deposited on fluorine doped tin oxide (FTO) substrates using hydrogen (H_2, 65 sccm) and methane (CH_4, 50 sccm) through hot filament chemical vapor deposition (HFCVD) technique. The vertically aligned ZnO NRs were applied as effective photoanode for the fabrication of efficient dye sensitized solar cells (DSSCs). Highly uniform ZnO NRs were grown on GO deposited FTO substrate with the average length of ~2−4 μm and diameter of ~200−300 nm. The possible mechanism of grown ZnO NRs clearly revealed the significant role of GO on FTO in architecting the aligned growth of ZnO NRs. The grown vertically aligned ZnO NRs possessed a typical wurtzite hexagonal crystal structure. The structural and the optical studies confirmed the formation of partial hydrogen bonding between surface functional groups of GO and ZnO NRs. A solar-to-electricity conversion efficiency of ~2.5% was achieved by DSSC fabricated with ZnO NRs deposited on graphene oxide (GO-ZnO NRs) thin film photoanode. The presence of GO on FTO substrate expressively increased the surface area of GO-ZnO photoanode, which resulted in high dye loading as well as high light harvesting efficiency and thus ensued the increased photocurrent density and the improved performance of DSSCs.

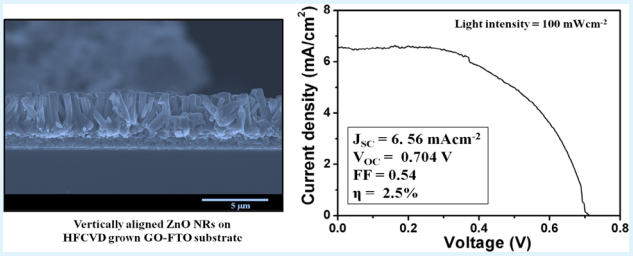

KEYWORDS: *graphene oxide, hot filament, carbon nanomaterials, thin film, zinc oxide nanorods, photoanode*

INTRODUCTION

A next-generation photovoltaic device named as dye sensitized solar cells (DSSCs) has been recently receiving great interest due to its reasonably high solar-to-electricity conversion efficiency with very low manufacturing cost.[1,2] In typical DSSC, the dye absorbed semiconducting electrode is an important component for the electron injection via absorption of photons from light. The surface and the electronic properties of semiconducting electrode are crucial for improving the photocurrent density and the conversion efficiency of DSSCs.[3] The absorption, electronic and the interfacial properties of photoanodes could be improved by controlling the structures, particle sizes and the textures of the photoanode.[4] Moreover, these factors could also elevate the solar-to-electricity conversion efficiency and diminishes the recombination rate at the interface of the semiconducting material and the electrolyte layer.[5] Various semiconducting metal oxides like SnO_2,[6] In_2O_3, Nb_2O_5[7] and ZnO[8,9] have been widely used as promising thin film photoanode materials for DSSCs. ZnO has wide band gap (3.44 eV),[10] high exciton binding energy (60 meV), high electronic mobility[11−13] and thus, actively explored as an alternative anode material in DSSCs. Importantly, the nanostructures of ZnO could be easily tailored by using different methods. The aligned ZnO nanostructures, such as nanowires (NWs), nanorods (NRs), nanobelts (NBs, and nanotubes (NTs) are being grown because of their good electrical conductivity and high surface-to-volume ratio for high absorption of dye molecules, improved light absorption, and application of p−n junctions and photovoltaic devices.[14,15] Among these, the vertically aligned ZnO NWs and NRs are substantial photoanode materials because of their high surface-to-volume ratio and the good electrical characteristics.[16,17]

Graphene as a 2D carbon-based material is applied enormously in electronic applications because of its good conductivity, superior chemical stability, large surface-to-volume ratio, and suitable pore size distribution.[18] The incorporation of graphene into polymer,[19,20] ceramic materials[21] and metal oxides remarkably improves the optoelectrical and electrochemical properties of the host materials. Few literatures are available on the growth of ZnO nanostructures on graphene based substrates and their application in solar devices.[22−24] Hwang and Kim et al[25,26] recently demonstrated the flexible optoelectronic hybrid material using ZnO nanostructures on graphene sheets. Chang et al.[27] reported

Received: June 14, 2012
Accepted: July 24, 2012
Published: July 24, 2012

 © 2012 American Chemical Society

the preparation of ZnO-graphene heterostructure on various substrates by a seeded solution method. To the best of our knowledge, no report is available on the growth of vertically aligned ZnO on the surface of GO-FTO substrates in which GO thin film is directly grown on FTO substrate by HFCVD technique. In this work, the vertically aligned ZnO NRs are grown by the low temperature hydrothermal method on GO coated FTO substrates and applied as photoanode for the application of DSSCs. The direct coating of GO on FTO substrate is carried out through HFCVD with the introduction of hydrogen (H_2, 65 sccm) and methane (CH_4, 50 sccm) in a chamber. The GO-ZnO NRs photoanode delivers the solar-to-electricity conversion efficiency of ∼2.5% with enhanced J_{SC}, V_{OC}, and FF.

EXPERIMENTAL SECTION

Synthesis of GO Thin Film on FTO. The cleaned fluorinated tin oxide glass (FTO glass, Hartford Glass Co., 8 Ω/sq, 80% transmittance in visible spectrum) substrates were used for the direct deposition of GO thin film by HFCVD technique, using a mixture of methane (CH_4) and hydrogen (H_2) gases. In brief, the FTO substrate was introduced into the HFCVD chamber and annealed in the presence of H_2 (65 sccm) for 30 min. Further annealing was performed by continuing H_2 with same flow rate, at the filament temperature of 1200 °C for 5 min to remove the traces of organic materials and oxide layers from the substrate. Finally, the methane (CH_4, 50 sccm) as a carbon precursor was introduced into the reactor for 5 min to produce a thin layer of GO on the FTO substrate and the system was allowed to cool at room temperature by passing argon (Ar, 200 sccm) for 90 min. The obtained GO thin film on FTO (GO-FTO) substrates was used for the deposition of vertically aligned ZnO NRs.

Synthesis of Vertically Aligned ZnO NRs on GO-Coated FTO. The vertically aligned ZnO NRs were grown by the hydrothermal method using HFCVD deposited GO-FTO substrate. Typically, an aqueous equimolar (0.1 M) reaction mixture of zinc nitrate hexahydrate ($Zn(NO_3)_2{\cdot}6H_2O$, Aldrich−Sigma, 98% assay) and hexamethylenetetramine ($(CH_2)_6N_4$, HMTA, Aldrich−Sigma, 98% assay) was prepared. The prepared GO-FTO substrates were placed upside down into the Teflon beaker and transferred to the stainless steel autoclaves and maintained at the temperature at 85 °C for 3 h. After completion of the reaction, the vertically aligned ZnO NRs grown on GO-FTO (GO-ZnO NRs) substrates were taken out and washed with deionized (DI) water and methanol. The grown GO-ZnO NRs were dried at 90 °C for 3 h to remove the residual materials.

Fabrication of GO-ZnO NRs Photoanode-Based DSSCs. For the fabrication of DSSC, the grown GO-ZnO NRs substrates were immersed in the ethanolic solution of ruthenium(II) 535 bis-TBA (0.3 mM, N-719, Solaronix) dye for 12 h at the room temperature under dark conditions. The dye adsorbed thin film electrodes were rinsed with absolute ethanol and dried under a nitrogen stream at 40 °C. The platinum (Pt)-coated FTO substrate as counter electrode was placed over the dye-adsorbed GO-ZnO NRs thin film electrode and the edges of the cell were sealed with 60 μm thick Surlyn sheet (SX 1170−60, Solaronix) by hot-pressing the two electrodes at 80 °C. An electrolyte of the specified composition (0.5 M LiI, 0.05 mM I_2, and 0.2 M tert-butyl pyridine in acetonitrile) was introduced through holes in the counter electrode using a syringe on the dye-immobilized thin film photoanode, and holes were sealed with small microscopic glass and Surlyn sheet.

Characterization. The morphology of the prepared GO-ZnO NRs thin film electrodes was observed by field emission scanning electron microscopy (FESEM, Hitachi S-4700) and transmission electron microscopy (TEM, H-7650, Hitachi, Japan). Crystalline structure of thin film electrodes was characterized by X-ray powder diffraction (XRD, Rigaku, Cu Kα, λ = 1.54178 Å) in the Bragg angle ranging between 10° and 80°. The structural modifications of GO-ZnO NRs thin film electrodes were studied by the Fourier transform infrared (FTIR, Nicolet, IR300) and Raman spectra (Raman microscope, Renishaw). UV−visible spectrophotometer (JASCO V-670) was used to obtain the absorption spectra of the samples over a range of 200−800 nm and Photoluminescence studies (JASCO, FP-6500) were used to characterize the optical properties of GO-ZnO NRs thin films. X-rays Photoelectron Spectroscopy (XPS) was performed by using AXIS-NOVA CJ109, Kratos Inc., ranges 0−800 eV for surface composition and the surface interaction of GO-ZnO NRs thin films. A current density (J)−voltage (V) curve was measured using a computerized digital multimeter (model 2000, Keithley) with a variable load. A 1000 W metal halide lamp served as a light source, and its light intensity was adjusted to simulated AM 1.5 at 100 mW cm^{-2} with a Si photo detector fitted with a KG-5 filter as a reference, calibrated at NREL, USA. A black tape mask was placed on top of the cell during the J−V measurements. The incident photon-to-current conversion efficiency (IPCE) as a function of wavelength was measured with a 150 W Xe lamp in combination with a 520 nm monochromator and a Keithley 236 source measure unit was controlled by the computer software.

RESULTS AND DISCUSSION

Figure 1 shows the cross section and surface FESEM images of HFCVD grown GO-FTO and ZnO-GO thin film substrates.

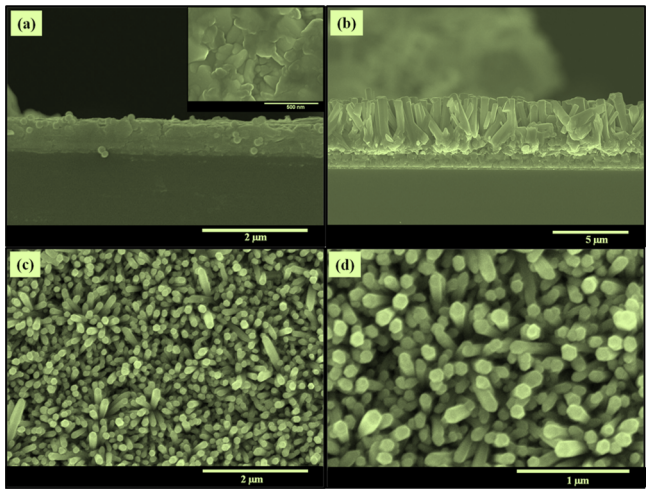

Figure 1. Cross-sectional FESEM images of (a) GO-FTO and (b) GO-ZnO NRs thin film. Surface FESEM images of GO-ZnO NRs thin film at (c) low magnification and (d) high magnification. Inset shows the surface view of GO-FTO thin film.

The GO sheets are deposited and uniformly arranged on the FTO substrate with the GO thickness of ∼600 nm, as shown in Figure 1a. Figure 1b demonstrates that the ZnO NRs are vertically aligned on the GO-FTO thin film. ZnO NRs exhibits the average length of ∼2−4 μm and obtains the average thickness of ∼5 μm including the GO thin layer. The surface images clearly show that ZnO NRs are highly dense and grown vertically on GO-FTO substrates, as shown in Figure 1(c, d). The high resolution image (Figure 1d) reveals that the obtained ZnO NRs possess hexagonal morphology with average diameter of ∼200−300 nm. The elemental composition and distribution in ZnO NRs are examined by the elemental mapping images of Zn and O elements, as shown in Figure 2. These mapping images reveal the homogeneous distribution of the Zn and O elements in ZnO NRs.

Figure 3 shows the transmission electron microscopy (TEM), high-resolution (HR) TEM, fast Fourier transform (FFT) of HRTEM and a selected area electron pattern (SAED)

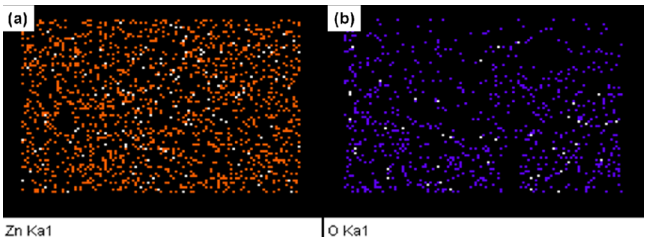

Figure 2. Elemental mapping of (a) Zn and (b) O for FESEM image of Figure 1d.

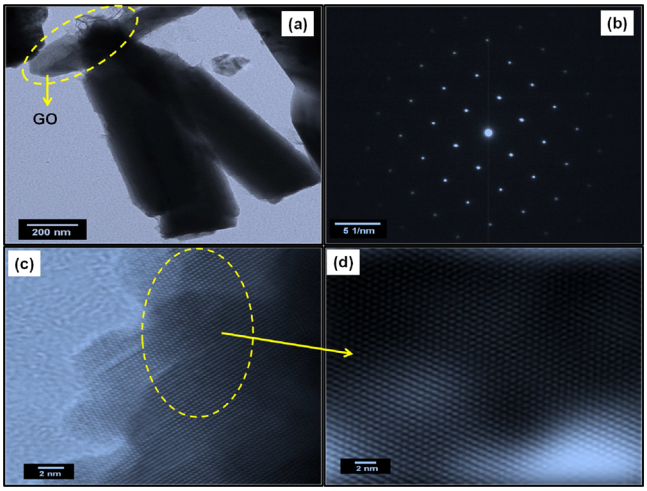

Figure 3. (a) TEM image, (b) SAED pattern, (c) HR-TEM, and (d) corresponding FFT of GO-ZnO NRs thin film.

of GO-ZnO NRs. Similar to FESEM images, Figure 3a deduces the morphology of ZnO NRs with the diameter and length of ∼200−300 nm and ∼2−4 μm, respectively. It is noticed that the sheets morphology are seen at the end of ZnO NRs which suggests the presence of GO layer in GO-ZnO NRs substrates. The grown GO-ZnO NRs show the typical pattern of a wurtzite single-crystal ZnO with preferentially grown in (0001) direction, as observed in SAED patterns (Figure 3b). Furthermore, the HRTEM image (Figure 3c) of ZnO NRs present well-resolved lattice fringes of crystalline ZnO NRs with the interplanar spacing of ∼0.52 nm which is well indexed with the lattice constant in the reference (JCPDS No. 36−1451). The FFT of HRTEM (Figure 3(d)) again confirms the interplanar spacing of two adjacent fringes of ZnO NRs. Additionally, this value corresponds to the *d*-spacing of (0001) crystal planes of wurtzite ZnO. Thus, the grown vertically aligned ZnO NRs is a single crystal and preferentially grown along the *c*-axis (0001).

Figure 4a shows the XRD patterns of GO-FTO and GO-ZnO NRs thin film substrates. The GO thin film shows a broad diffraction peak centered at 17.87 Å, which is attributed to the characteristic peaks of graphene sheets. However, the GO-ZnO NRs exhibits the diffraction peaks at ∼31.7, ∼34.2, ∼36.1, ∼47.4, ∼56.5, 67.8, and ∼68.9°, representing the typical hexagonal wurtzite structure of ZnO NRs which is well indexed with the hexagonal wurtzite ZnO structure of JCPDS 36−1451. The small broader diffraction peak at ∼10−20° is observed in the GO-ZnO NRs, which is similar to the diffraction patterns of GO thin film. Moreover, the diffraction peaks at ∼26.3, ∼54.4, and ∼62.6° correspond to the FTO layer of the glass.[28] Thus, the strong and sharp characteristics peaks of ZnO with very

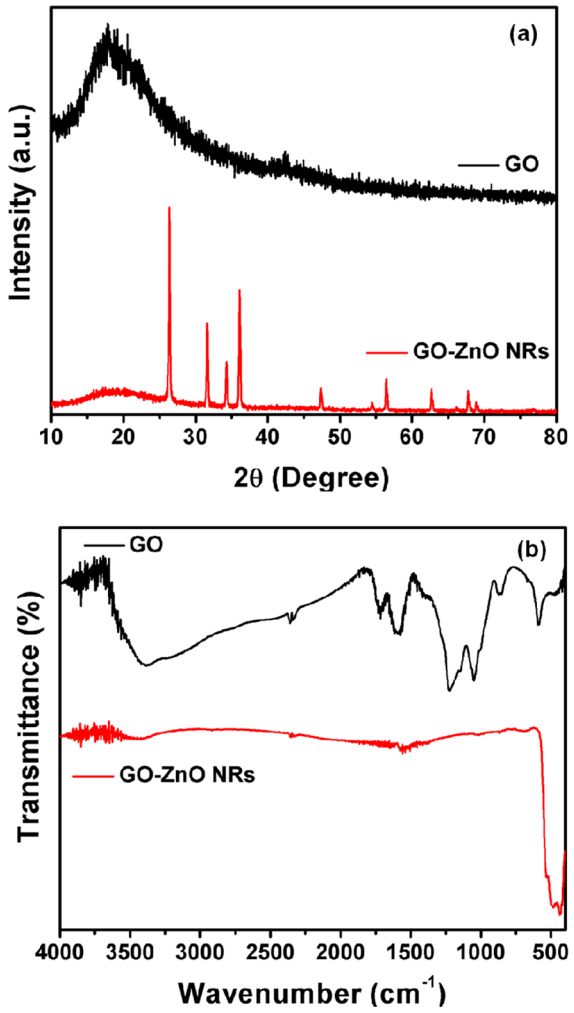

Figure 4. (a) XRD pattern and (b) FTIR spectra of GO-FTO and GO-ZnO NRs thin film.

weak broad GO peak in GO-ZnO NRs thin film suggest the high crystallinity of grown ZnO NRs on the GO-FTO substrate. The structural investigations of GO-FTO and GO-ZnO thin films are analyzed by the FTIR spectroscopy, as shown in Figure 4b. The HFCVD grown GO-FTO thin film presents the IR bands at ∼3390, ∼1054, ∼1220, and ∼1721 cm^{-1}, which correspond to −OH stretching vibrations, C−O stretching vibrations, C−OH stretching peak, and C═O stretching of COOH groups, respectively.[29] The presence of these characteristics bands suggests the oxygen-containing functional groups on GO-FTO thin film. The peaks at ∼1589 cm^{-1} indicates the skeletal vibration of GO.[30] In GO-ZnO NRs thin film, the strong ZnO band at ∼495 cm^{-1} is associated to the characteristic peak of the Zn−O stretching vibration of bulk ZnO,[28] and the reduced peak intensities of GO confirm the presence of ZnO and GO layer.

The Raman spectra of GO thin film and GO-ZnO NRs thin film are shown in Figure 5. HFCVD grown GO thin film shows two Raman shifts at ∼1348 cm^{-1} and ∼1592 cm^{-1}, correspond to D and G bands respectively, as shown in Figure 5b. In general, the G band and D band represent the breathing mode of κ-point phonons of A_{1g} symmetry and the E_{2g} phonon of C sp^2 atoms, respectively.[31] The lower D Raman band originates from the structural defects due to the presence of the hydroxyl and epoxide groups on the carbon basal plane.[32] However, GO-

dx.doi.org/10.1021/am301064j | ACS Appl. Mater. Interfaces 2012, 4, 4405−4412

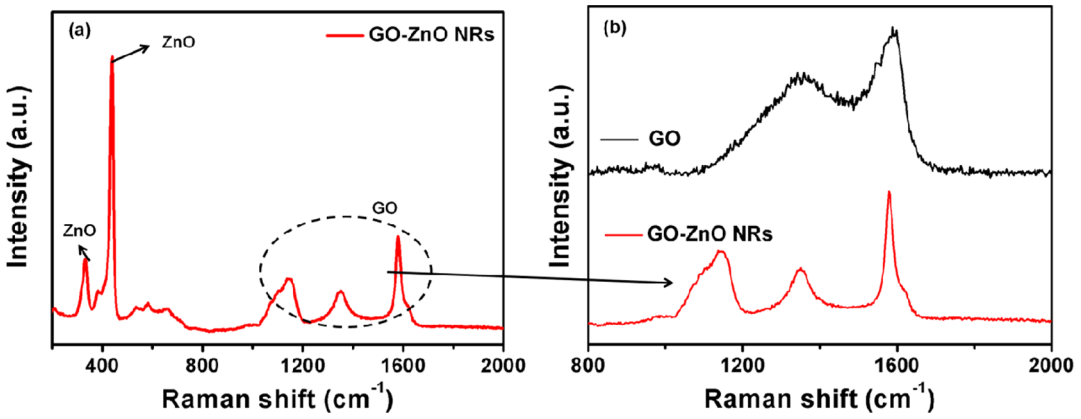

Figure 5. Raman spectra of (a) GO-ZnO NRs thin film and (b) a part of Raman spectra of GO-ZnO NRs and GO-FTO thin film in the range of 1000−2000 cm^{-1}.

ZnO NRs thin film (Figure 5a) possesses similar nature of D and G along with three Raman shifts at ∼331.4, ∼437, and ∼587 cm^{-1}. The strong Raman shift at ∼437 cm^{-1} is assigned to E_2 mode of ZnO E_2 mode of ZnO crystal, which is consistent with Raman peak of bulk ZnO crystals.[33] The two small peaks at ∼331 cm^{-1} and ∼587 cm^{-1} are designated to the second order Raman spectrum arising from zone-boundary phonons $3E_{2H}-E_{2\,L}$ for wurtzite hexagonal ZnO single crystals and E_1 (LO) mode of ZnO associated with oxygen deficiency in ZnO nanomaterials respectively.[34] It is estimated that the I_D/I_G of GO thin film is 0.848 which significantly decreases to 0.601 for GO-ZnO NRs thin film. It suggests that most of the oxygenated groups on the carbon basal plane in GO thin film might interact with surface hydroxyl groups of ZnO NRs.

Figure 6a shows the UV−vis absorption spectra of the GO and GO-ZnO NRs thin film, obtained by dispersing both the samples in ethanol. A small absorption peak at ∼264 nm in the UV−vis absorption spectra of GO is ascribed to typical π-plasmon of graphitic structure.[35] The GO-ZnO NRs thin film exhibits the strong absorption peak at ∼382 nm, revealing the existence of the crystalline wurtzite hexagonal ZnO.[36] A significant shift of absorption peak to the visible region is noticed for GO-ZnO NRs thin film, which might arise from the increase of the surface electric charge of the oxides in the GO-ZnO NRs thin film.[37] Moreover, the disappearance of GO in the GO-ZnO NRs thin film might occur due to the high crystalline nature of the vertically aligned ZnO NRs on GO-FTO substrate. Figure 6b depicts the PL spectra of GO-ZnO NRs thin film at room temperature. The PL of GO-ZnO NRs exhibits a sharp emission at ∼381 nm, corresponding to the near band edge emission.[38] A large and broad green emission at ∼572 nm is represented to free exciton emission from the wide band gap of ZnO NRs and the recombination of electrons in the single occupied oxygen vacancies in ZnO nanomaterials.[39] Importantly, the presence of large green emission with same intensity of UV emission might also originate from the interaction of oxygenated groups on GO thin film to the surface hydroxyl group of ZnO NRs, as shown in UV−vis studies (Figure 6a). Moreover, the sharp and strong UV emissions peaks of GO-ZnO NRs thin film also result from the high crystal quality of ZnO NRs deposited on GO-FTO thin film. Thus, the highly dense vertically aligned ZnO NRs are uniformly grown on the GO-FTO substrate because of the interaction between GO and ZnO NRs.

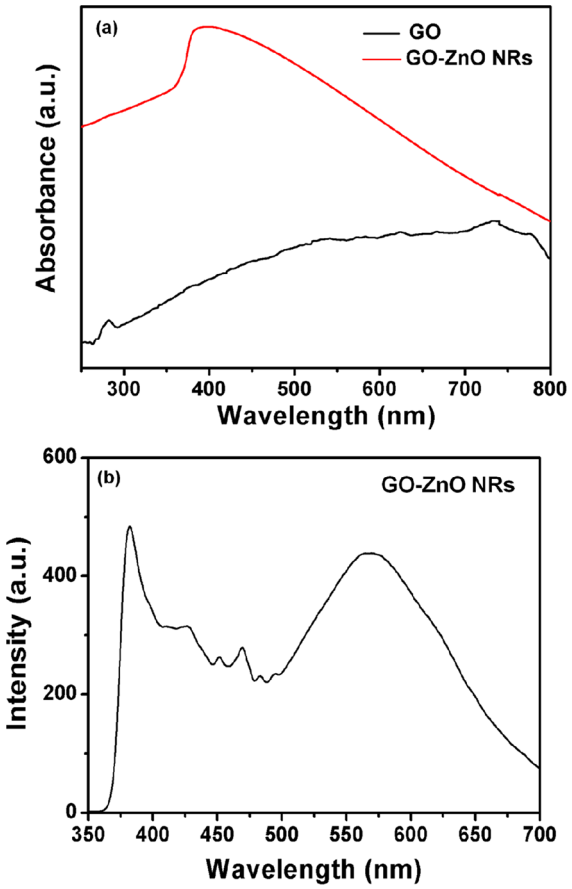

Figure 6. (a) UV−vis spectra and (b) photoluminescence spectra of GO-FTO and GO-ZnO NRs thin film.

The chemical states of GO-ZnO NRs thin film are analyzed by the XPS spectra as shown in Figure 7. The survey spectrum (Figure 7a) shows the peaks of C 1s, Zn 2p, and O 1s for the GO-ZnO NRs. The deconvoluted C1s XPS spectra of the GO-ZnO NRs are comprised of five peaks, as depicted in Figure 7(b). The binding energies at ∼285.3 eV is assigned to C−C and C═C/C−H bonds. Other binding energies at ∼286.3 eV, ∼287.2 eV and ∼288.2 eV represent the C−OH, C═O and −O−C═O bonds, respectively.[40] The appearance of binding energy at ∼283.7 eV might arise from the C−O−M bond,[41] suggesting the formation of bond between C and Zn in the GO-ZnO as reported elsewhere.[42] In Figure 7c, two binding

dx.doi.org/10.1021/am301064j | ACS Appl. Mater. Interfaces 2012, 4, 4405−4412

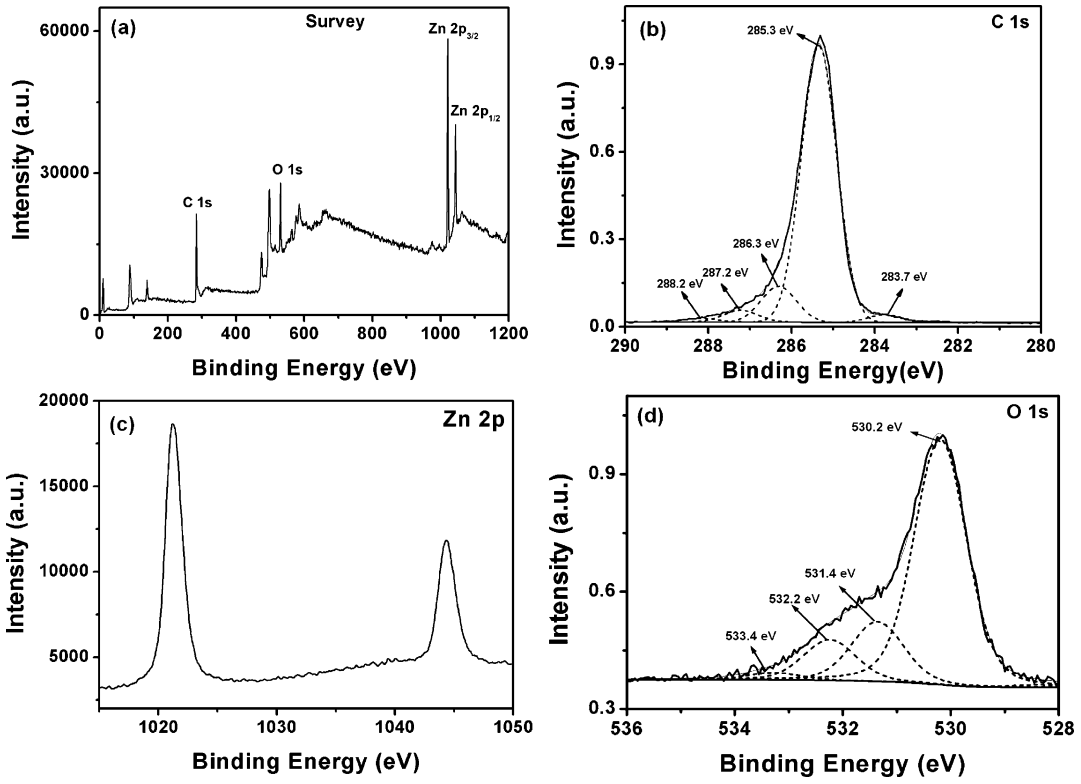

Figure 7. XPS spectra of (a) survey, (b) C 1s, (c) Zn 2p, and (d) O 1s of GO-ZnO NRs thin film.

energies peaks at ~1021 eV and ~1044 eV are observed in the Zn 2p XPS spectra, corresponding to the Zn $2p_{3/2}$ and Zn $2p_{1/2}$, respectively. The binding energies are slightly lower than the binding energies of the Zn 2p core level of bulk ZnO (~1022 eV and ~1046 eV),[43] which reveal the interaction between GO and ZnO NRs. Figure 7(d) displays the four deconvoluted peaks at ~530.2, ~531.4, ~532.2, and weak peak at ~533.4 eV. The main binding energy peak at ~530.2 eV is attributed to the O ion of ZnO lattice, however other two peaks at ~531.4 and ~532.2 eV are associated to the surface oxygenated species such as C−O or O−H and the adsorbed H_2O, respectively. The appearance of C−O bond again confirms the interaction between GO and ZnO NRs. Thus, the grown ZnO NRs are significantly attached on the GO layer via the bonding between GO and ZnO.

A possible mechanism is proposed for the growth of vertically aligned ZnO NRs on GO-FTO substrates, as schematically illustrated in Figure 8. First, GO thin layer is deposited on FTO substrates through HFCVD technique by using CH_4 and H_2 gases. The growth of GO thin film by HFCVD basically involves the three steps i.e. vaporization, nucleation and condensation.[44] In our case, the FTO glass substrate is placed into HFCVD chamber and then the annealing in the presence of H_2 (65 sccm) for 30 min is performed to avoid any effect or reaction of oxygenated species to reacting species. Thereafter, the CH_4 gas as precursor source is flowed which first adsorbs on the surface of FTO and second, the expansion of deposition might occur by increasing the filament temperature up to 1200 °C. Generally, the FTO layer on glass substrate produces the high roughness on the substrate. It is reported that the use of conducting substrate with highly rough or scratched surface provides the enough surface for the growth of carbon thin film.[45] Herein, the rough surface of FTO substrates might increase the nucleation of

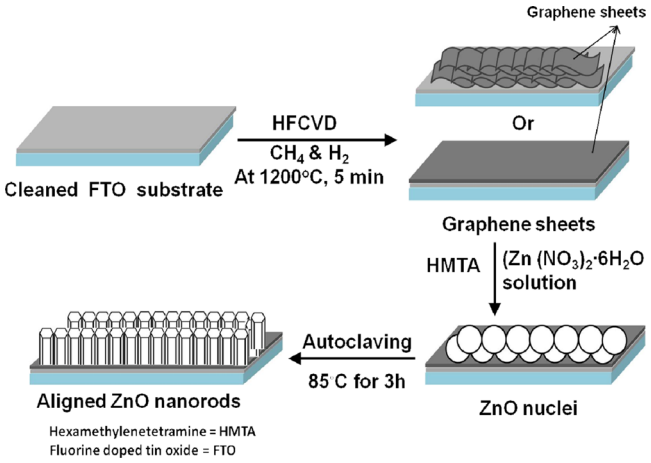

Figure 8. Possible growth mechanism of GO-ZnO NRs thin film.

carbon deposition by decreasing the surface energy which might helpful for the layer by layer deposition of carbon on FTO substrates, as shown in Figure 1a. It is reported that the hydroxyl and epoxy functional groups are present on the basal planes of GO whereas, the carbonyl and carboxyl groups at the edges of GO sheet.[46] These surface species are very active on the GO thin film and tends to adsorb the positive metal ions (Zn^{2+}) and salts.[47] In our experiment, the GO-FTO substrates are immersed in the aqueous solution of Zn $(NO_3)_2$ (as Zn source) and HMT (as OH^- source). Reactions 1 and 2 present the formation of OH^- from the HMT molecule. At first, the reaction 1 decomposes HMT into HCHO and NH_3 and afterward, (2) involves the reaction of NH_3 and H_2O to provide OH^- ions upon slow heating. The OH^- ions reacts with Zn^{2+} from $Zn(NO)_3$ at the elevated temperature to generate

dx.doi.org/10.1021/am301064j | ACS Appl. Mater. Interfaces 2012, 4, 4405−4412

$Zn(OH)_2$, and subsequently the dehydration of $Zn(OH)_2$ forms ZnO nuclei on the GO-FTO substrate, as expressed in reactions 3 and 4

$$(CH_2)_6N_4 + 6H_2O \rightarrow 6HCHO + 4NH_3 \quad (1)$$

$$NH_3 + H_2O \rightarrow NH_4^+ + OH^- \quad (2)$$

$$Zn^{2+} + 2OH^- \rightarrow Zn(OH)_2 \quad (3)$$

$$2Zn(OH)_2 \rightarrow ZnO + H_2O + 2OH^- \quad (4)$$

The schematic illustration defines the growth of vertically aligned ZnO NRs on the GO-FTO substrate. The adsorbed Zn^{2+} ions provide the spherical ZnO nuclei with the reaction of OH^- ions. Zn atoms of ZnO nuclei might create the bonding between O atoms of the functional groups on GO layer via a covalent coordination bond, which might act as the nucleation center for the growth of ZnO crystals. At the elevated temperature with prolonged time, the ZnO nuclei become larger along the planes and the edges to originate the hexagonal structure on the GO-FTO substrate. Moreover, like the seeded FTO substrates, the GO layer might decrease the surface energy between ZnO nuclei and FTO substrate, which simplifies the growth pathway for the upstanding or upward structures. Thus, the highly dense vertically aligned ZnO NRs are formed on the surface of the GO-FTO substrates.

Figure 9a shows the current density−voltage (J−V) characteristics of DSSCs fabricated with GO-ZnO NRs photoanode under 100 mW cm^{-2} light intensity (1.5AM). DSSC fabricated with GO-ZnO NRs thin film photoanode exhibits the moderate conversion efficiency (η) of ∼2.5% with a high short circuit current (J_{SC}) of ∼6.56 mA cm^{-2}, open circuit voltage (V_{OC}) of ∼0.704 V, and fill factor (FF) of 0.54. However, the aligned ZnO NR-based DSSC has recorded the relatively inferior conversion efficiency of ∼1.18% with J_{SC} of ∼3.45 $mAcm^{-1}$, V_{OC} of ∼0.591 V, and FF of ∼0.58, as presented in Table 1. Moreover, the photocurrent density and the conversion efficiency have significantly improved than the other reported DSSCs, fabricated with aligned ZnO NRs photoanodes grown by the solution methods.[48−51] The better photovoltaic properties might associate with the highly dense uniform aligned nanorods, existence of GO layer and the increased optical properties, which collectively results to the high absorption of dye and light harvesting efficiency. Additionally, the contact area between GO layer and ZnO NRs might provide larger surface area of 29.4 $m^2 g^{-1}$ for absorbing dye molecules and make a better pathway for the fast electron transfer. Thus, the improved photovoltaic properties of DSSC with GO-ZnO NRs photoanode is attributed to sufficiently high surface area, dye absorption and light harvesting efficiency. It is studied that ZnO photoanodes with aligned morphology like NRs, NTs arrays increases the charge collection and transfer properties.[52] It is also noticed that the synergistic effects might cause the reduction of the recombination rate and enhances the charge carrier collection and the transport rate. Moreover, the performance of DSSCs in terms of incident photon to current conversion (IPCE) efficiency is shown in Figure 9b. In principle, the IPCE is expressed by the ratio between the number of generated charge carriers contributing to the photocurrent and the number of incident photons, as expressed by eq 5

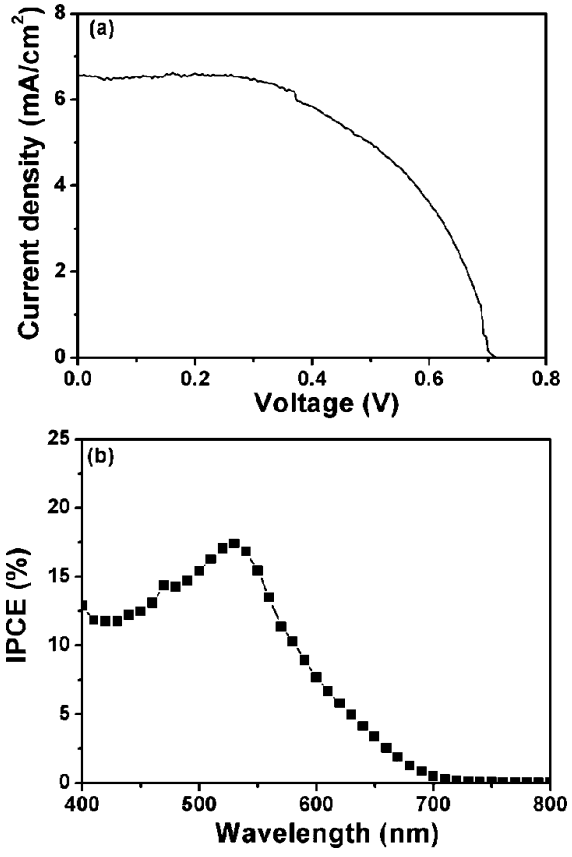

Figure 9. (a) J−V curve and (b) IPCE curve of the DSSCs fabricated with GO-ZnO NRs thin film photoanode.

Table 1. Summary of Photovoltaic Performances of Fabricated DSSCs

		J−V curves summary			
photoanodes aligned ZnO NRs	IPCE (%)	J_{SC} ($mAcm^{-2}$)	V_{OC} (V)	FF	η (%)
FTO/ZnO	14.2	3.45	0.591	0.58	1.18
FTO/GO-ZnO	17.8	6.56	0.704	0.54	2.5

$$\text{IPCE}\ (\%) = 1240 J_{SC}(\mu A\ cm^{-2})/\lambda(nm) P_{in}(mW\ cm^{-2}) \times 100 \quad (5)$$

Where J_{SC} is the short-circuit photocurrent density for monochromatic incident light and λ and P_{in} are the wavelength and the intensity of the monochromatic light, respectively. DSSC fabricated with GO-ZnO NRs photoanode shows a maximum IPCE value of ∼17.8% at the absorption wavelength of ∼530 nm. As discussed above, the presence of GO layer has significantly enhanced the surface area of GO-ZnO NRs photoanode and dye absorption through the good interfacial contact between GO-ZnO layer and FTO layer, resulting in the reasonably high IPCE. Thus, the enhanced IPCE of GO-ZnO NRs photoanode based DSSC are resulted from the high J_{SC}, V_{OC}, and the improved photovoltaic performances.

CONCLUSIONS

The vertically aligned ZnO NRs are grown on HFCVD deposited GO-FTO substrates by the low temperature hydrothermal method and applied as photoanode for the fabrication of efficient DSSCs. The uniform vertically aligned

ZnO NRs on GO-FTO substrates are highly crystalline with typical wurtzite hexagonal crystal structure. By the structural, surface and optical studies, a partial hydrogen bonding between surface functional groups of GO and ZnO NRs confirms the role of GO layer in the formation of aligned ZnO NRs. A solar-to-electricity conversion efficiency of ~2.5% with J_{SC} of ~6.56 $mAcm^{-2}$, V_{OC} of ~0.71 V and FF of ~0.54 are achieved by DSSC fabricated with GO-ZnO NRs thin film photoanode. The presence of GO on FTO substrate substantially increases the surface area of GO-ZnO photoanode, which tends to high dye loading as well as high light harvesting efficiency and thus, results to the increased photocurrent density and the performance of DSSCs.

AUTHOR INFORMATION

Corresponding Author

*Tel: +82-63-270-2438. Fax: +82 63 270 2306. E-mail addre: hsshin@jbnu.ac.kr (H.S.S.).

Author Contributions

†These authors contributed equally to this work.

Notes

The authors declare no competing financial interest.

ACKNOWLEDGMENTS

Dr. Sadia Ameen gratefully acknowledges the post doctoral fellowship granted by National Research Foundation (NRF 2011) for foreign researchers. This work is fully supported by NRF Project # 2011-0029527 and the Research Funds of Chonbuk National University in 2009. We would like to thank Mr. Kang Jong-Gyun, Center for University-Wide Research Facilities, Chonbuk National University for his cooperation in TEM images.

REFERENCES

(1) Chiba, Y.; Islam, A.; Watanabe, Y.; Komiya, R.; Koide, N.; Han, L. Y. *J. Appl. Phys.* **2006**, *45*, L638−L640.

(2) Wang, Z. S.; Yanagida, M.; Sayama, K.; Sugihara, H. *Chem. Mater.* **2006**, *18*, 2912−2916.

(3) Grätzel, M. *J. Photochem. Photobiol. C* **2003**, *4*, 145−153.

(4) Ito, S.; Kitamura, T.; Wada, Y.; Yanagida, S. *Sol. Energy. Mater. Sol. Cell* **2003**, *76*, 3−13.

(5) Kim, S. S.; Yum, J. H.; Sung, Y. E. *J. Photochem. Photobiol. Chem* **2005**, *171*, 269−273.

(6) Katoh, R.; Furube, A.; Yoshihara, T.; Hara, K.; Fujihashi, G.; Takano, S. *J. Phys. Chem. B* **2004**, *108*, 4818−4822.

(7) Sayama, K.; Sugihara, H.; Arakawa, H. *Chem, Mater* **1998**, *10*, 3825−3832.

(8) Zhang, Q. F.; Chou, T. P.; Russo, B.; Jenekhe, S. A.; Cao, G. Z. *Angew. Chem., Int. Ed.* **2008**, *47*, 2402−2406.

(9) Hsu, Y. F.; Xi, Y. Y.; Yip, C. T.; Djurisi, A. B.; Chan, W. K. *J. Appl. Phys.* **2008**, *10*, 083114−083117.

(10) Baskoutas, S.; Bester, G. *J. Phys. Chem. C* **2010**, *114*, 9301−9307.

(11) Tabatabaee, M.; Mirrahimi, S. A. *Orient J. Chem.* **2011**, *27*, 64−68.

(12) Zhang, H.; Du, N.; Chen, B.; Li, D.; Yang, D. *Sci. Adv. Mater.* **2009**, *1*, 13−17.

(13) Jafari, A.; Ghane, M.; Sarabi, M.; Siyavoshifar, F. *Orient J. Chem.* **2011**, *27*, 811−822.

(14) Galoppini, E.; Rochford, J.; Chen, H.; Lu, G. Y.; Hagfeldt, A.; Boschloo, G. *J. Phys. Chem. B* **2006**, *110*, 16159−16161.

(15) Gao, Y. F.; Nagai, M.; Chang, T. C.; Shyue, J. *J. Cryst. Growth. Des.* **2007**, *7*, 2467−2471.

(16) Chrissanthopoulos, A.; Baskoutas, S.; Bouropoulos, N.; Dracopoulos, V.; Poulopoulos, P.; Yannopoulos, S. N. *Photonics Nanostruct. Fundam. Appl.* **2011**, *9*, 132−139.

(17) Galoppini, E.; Rochford, J.; Chen, H. H.; Saraf, G.; Lu, Y. C.; Hagfeldt, A.; Boschloo, G. *J Phys. Chem. C* **2006**, *110*, 16159−16161.

(18) Lu, T.; Zhang, Y.; Li, H.; Pan, L.; Li, Y.; Sun, Z. *Electrochim. Acta* **2010**, *55*, 4170−4173.

(19) Liu, N.; Luo, F.; Wu, H. X.; Liu, Y. H.; Zhang, C. J. *Adv. Funct. Mater.* **2008**, *18*, 1518−1525.

(20) Eda, G.; Chhowalla, M. *Nano Lett.* **2009**, *9*, 814−818.

(21) Watcharotone, S. D.; Dikin, A.; Stankovich, S.; Piner, R.; Jung, I.; Dommett, G. H. B.; Evmenenko, G.; Wu, S. E.; Chen, S.; Liu, C. P.; Nguyen, S. T.; Ruoff, R. S. *Nano Lett.* **2007**, *7*, 1888−1892.

(22) Kim, Y. J.; Hadiyawarman, Y. A.; Kim, M.; Y, i G. C.; Liu, C. *Nanotechnology* **2011**, *22*, 245603−245608.

(23) Chen, J.; Li, C.; Ed., G.; Zhang, Y.; Lei, W.; Chhowalla, M.; Milne, W. I.; Deng, W. Q. *Chem. Commun.* **2011**, *47*, 6084−6086.

(24) Yin, Z.; Wu, S.; Zhou, X.; Huang, X.; Zhang, Q.; Boey, F.; Zhang, H. *Small* **2010**, *6*, 307−312.

(25) Hwang, J. O.; Lee, D. H.; Kim, J. Y. T.; Han, H.; Kim, B. H.; Park, M.; No, K.; Kim, S. O. *J. Mater. Chem.* **2010**, *21*, 3432−3437.

(26) Yang, Y.; Liu, T. *Appl. Surf. Sci.* **2011**, *257*, 8950−8954.

(27) Chang, H. X.; Sun, Z. H.; Ho, K. Y. F.; Tao, X. M.; Yan, F.; Kwok, W. M.; Zheng, Z. J. *Nanoscale* **2011**, *3*, 258−264.

(28) Ameen, S.; Akhtar, M. S.; Ansari, S. G.; Yang, O. B.; Shin, H. S. *Superlatt. Microstruct.* **2009**, *46*, 872−880.

(29) Xu, Y. X.; Bai, H.; Lu, G. W.; Li, C.; Shi, G. Q. *J. Am. Chem. Soc.* **2008**, *130*, 5856−5857.

(30) Wu, J.; Shen, X.; Jiang, L.; Wang, K.; Chen, K. *Appl. Surf. Sci.* **2010**, *256*, 2826−2830.

(31) Guo, M.; Diao, P.; Wang, X.; Cai, S. *J. Solid State Chem.* **2005**, *178*, 3210−3215.

(32) Alvera, U.; Zhou, W.; Belay, A. B.; Krueger, R.; Davis, K. O.; Hickman, N. S. *Appl. Surf. Sci.* **2012**, *258*, 3109−3114.

(33) Roy, C.; Byrne, S.; McGlynn, E.; Mosnier, J. P.; Posada, Ede.; Mahony, D. O.; Lunney, J. G.; Henry, M. O.; Ryan, B.; Cafolla, A. A. *Thin Solid Films* **2003**, *436*, 273−276.

(34) Exarhos, G.; Sharma, S. K. *Thin Solid Films* **1995**, *270*, 27−32.

(35) Wang, X.; Zhi, L. J.; Tsao, N.; Tomovic, J. L.; Mullen, K. *Angew. Chem., Int. Ed.* **2008**, *47*, 2990−2992.

(36) Xing, L.; Zhang, X. *J. Phys. Chem. C* **2007**, *111*, 9081−9085.

(37) Lv, T.; Pan, L.; Liu, X.; Lu, T.; Zhu, G.; Sun, Z. *J. Alloys Compd.* **2011**, *509*, 10086−10091.

(38) Cuong, T. V.; Pham, V. H.; Chung, J. S.; Shin, E.; Woo.; Hahn, S. H.; Huh, J. S.; Rue, G. H.; Kim, E. J.; Hur, S. H.; Kohl, P. A. *Mater. Lett.* **2010**, *64*, 2479−2482.

(39) Vanheusden, K.; Warren, W. L.; Seager, C. H.; Tallant, D. R.; Voigt, J. A.; Gnade, B. E. *J. Appl. Phys.* **1996**, *79*, 7983−7990.

(40) Yumitori, S. *J. Mater. Sci.* **2000**, *35*, 139−146.

(41) Fu, D.; Han, G.; Chang, Y.; Dong. *J. Mater. Chem. Phys.* **2012**, *132*, 673−681.

(42) Ameen, S.; Akhtar, M. S.; Kim, Y. S.; Yang, O. B.; Shin, H. S. *Microchim. Acta* **2011**, *172*, 471−478.

(43) Dreyer, D. R.; Park, S.; Bielawski, C. W.; Ruoff, R. S. *Chem. Soc. Rev.* **2010**, *39*, 228−240.

(44) Tillack, M. S.; Blair, D.; Harilal, S. S. *Nanotechnology* **2004**, *15*, 390−403.

(45) Dar, M. A.; Ansari, S. G.; Kim, Y. S.; Kim, G. S.; Seo, H. K.; Shin, J.; Kulkarni, S. K.; Shin, H. S. *Thin Solid Films* **2006**, *497*, 103−108.

(46) Bao, Q.; Zhang, D.; Qi, P. *J. Colloid Interface Sci.* **2011**, *360*, 463−470.

(47) Chrissanthopoulos, A.; Baskoutas, S.; Bouropoulos, N.; Dracopoulos, V.; Tasis, D.; Yannopoulos, S. N. *Thin Solid Films* **2007**, *515*, 8524−8528.

(48) Fu, Y. S.; Sun, J.; Xie, Y.; Liu, J.; Wang, H. L.; Du, X. W. *Mater. Sci. Eng., B* **2010**, *166*, 196−202.

(49) Yuan, K.; Yin, X.; Li, J.; Wu, J.; Wang, Y.; Huang, F. *J. Alloys Compd.* **2010**, *489*, 694−699.

(50) Hsu, Y. F.; Xi, Y. Y.; Djurišić, A. B.; Chan, W. K. *Appl. Phys. Lett.* **2008**, *92*, 133507−133509.
(51) Chung, J.; Lee, J.; Lim, S. *Phys. B: Condens. Matter.* **2010**, *405*, 2593−2598.
(52) Martinson, A. B. F.; Elam, J. W.; Hupp, J. T.; Pellin, M. J. *Nano Lett.* **2007**, *7*, 2183−2187.